



UNIVERSITY
OF WOLLONGONG
AUSTRALIA

University of Wollongong
Research Online

Australian Institute for Innovative Materials - Papers

Australian Institute for Innovative Materials

2017

Structural, electronic, magnetic, half-metallic, mechanical, and thermodynamic properties of the quaternary Heusler compound FeCrRuSi: A first-principles study

Xiaotian Wang

University of Wollongong, xw489@uowmail.edu.au

Houari Khachai

Universite Djillali Liabes de Sidi Bel Abbes

Rabah Khenata

Universite Mustapha Stambouli de Mascara

Hongkuan Yuan

Southwest University

LiYing Wang

Hebei University of Technology

See next page for additional authors

Publication Details

Wang, X., Khachai, H., Khenata, R., Yuan, H., Wang, L., Wang, W., Bouhemadou, A., Hao, L., Dai, X., Guo, R., Liu, G. & Cheng, Z. (2017). Structural, electronic, magnetic, half-metallic, mechanical, and thermodynamic properties of the quaternary Heusler compound FeCrRuSi: A first-principles study. *Scientific Reports*, 7 (1), 16183-1-16183-13.

Research Online is the open access institutional repository for the University of Wollongong. For further information contact the UOW Library: research-pubs@uow.edu.au

Structural, electronic, magnetic, half-metallic, mechanical, and thermodynamic properties of the quaternary Heusler compound FeCrRuSi: A first-principles study

Abstract

In this paper, we have investigated the structural, electronic, magnetic, half-metallic, mechanical, and thermodynamic properties of the equiatomic quaternary Heusler (EQH) compound FeCrRuSi using the density functional theory (DFT) and the quasi-harmonic Debye model. Our results reveal that FeCrRuSi is a half-metallic material (HMM) with a total magnetic moment of $2.0 \mu_B$ in agreement with the well-known Slater-Pauling rule $M_t = Z_t - 24$. Furthermore, the origin of the half-metallic band gap in FeCrRuSi is well studied through a schematic diagram of the possible d-d hybridization between Fe, Cr and Ru elements. The half-metallic behavior of FeCrRuSi can be maintained in a relatively wide range of variations of the lattice constant (5.5 - 5.8 \AA) under uniform strain and the c/a ratio (0.96 - 1.05) under tetragonal distortion. The calculated phonon dispersion, cohesive and formation energies, and mechanical properties reveal that FeCrRuSi is stable with an EQH structure. Importantly, the compound of interest has been prepared and is found to exist in an EQH type structure with the presence of some B2 disorder. Moreover, the thermodynamic properties, such as the thermal expansion coefficient α , the heat capacity C_V , the Grüneisen constant γ , and the Debye temperature Θ_D are calculated.


Publication Details

Wang, X., Khachai, H., Khenata, R., Yuan, H., Wang, L., Wang, W., Bouhemadou, A., Hao, L., Dai, X., Guo, R., Liu, G. & Cheng, Z. (2017). Structural, electronic, magnetic, half-metallic, mechanical, and thermodynamic properties of the quaternary Heusler compound FeCrRuSi: A first-principles study. *Scientific Reports*, 7 (1), 16183-1-16183-13.

Authors

Xiaotian Wang, Houari Khachai, Rabah Khenata, Hongkuan Yuan, LiYing Wang, Wenhong Wang, Abdelmadjid Bouhemadou, Liyu Hao, Xuefang Dai, Ruikang Guo, Guodong Liu, and Zhenxiang Cheng

SCIENTIFIC REPORTS



OPEN

Structural, electronic, magnetic, half-metallic, mechanical, and thermodynamic properties of the quaternary Heusler compound FeCrRuSi: A first-principles study

Xiaotian Wang^{1,2}, Houari Khachai³, Rabah Khenata⁴, Hongkuan Yuan¹, Liying Wang⁵, Wenhong Wang⁶, Abdelmadjid Bouhemadou⁷, Liyu Hao¹, Xuefang Dai⁵, Ruikang Guo⁵, Guodong Liu⁵ & Zhenxiang Cheng²

In this paper, we have investigated the structural, electronic, magnetic, half-metallic, mechanical, and thermodynamic properties of the equiatomic quaternary Heusler (EQH) compound FeCrRuSi using the density functional theory (DFT) and the quasi-harmonic Debye model. Our results reveal that FeCrRuSi is a half-metallic material (HMM) with a total magnetic moment of $2.0 \mu_B$ in agreement with the well-known Slater-Pauling rule $M_t = Z_t - 24$. Furthermore, the origin of the half-metallic band gap in FeCrRuSi is well studied through a schematic diagram of the possible *d-d* hybridization between Fe, Cr and Ru elements. The half-metallic behavior of FeCrRuSi can be maintained in a relatively wide range of variations of the lattice constant ($5.5\text{--}5.8 \text{ \AA}$) under uniform strain and the *c/a* ratio ($0.96\text{--}1.05$) under tetragonal distortion. The calculated phonon dispersion, cohesive and formation energies, and mechanical properties reveal that FeCrRuSi is stable with an EQH structure. Importantly, the compound of interest has been prepared and is found to exist in an EQH type structure with the presence of some B2 disorder. Moreover, the thermodynamic properties, such as the thermal expansion coefficient α , the heat capacity C_v , the Grüneisen constant γ , and the Debye temperature Θ_D are calculated.

In the field of magnetic materials, the topic of research about spintronics¹ has undoubtedly become of great concern. Furthermore, half-metallic materials (HMMs)² are attracting great attention recently because these type of materials provide novel functionalities in spintronic and magneto-electronic devices. The electronic structure of the HMMs is metallic in only one of the two spin channels, resulting in a 100% spin polarization of the electrons near the Fermi level. Among the HMMs based on different structures, the Heusler^{3–5} ones have a special importance because of their interesting physical properties, such as their high Curie temperatures and tunable electronic structure.

Several investigations^{6–16} on the HMMs based on equiatomic quaternary Heusler structure (EQH) (LiMgPdSn/Y structure, space group F-43m, #216), have been done. Compared with the pseudo ternary Heusler HMMs, the EQH ones have the advantage of lower power dissipation due to the lesser amount of disorder that exists in them¹⁷. In addition, Heusler-type thin films usually lose their predicted ultra-high spin polarization due

¹School of Physical Science and Technology, Southwest University, Chongqing, 400715, P.R. China. ²Institute for Superconducting & Electronic Materials (ISEM), University of Wollongong, Wollongong, 2500, Australia. ³Laboratoire d'Étude des Matériaux & Instrumentations Optiques; Département Matériaux & Développement Durable; Faculté des Sciences Exactes; Université Djillali Liabès de Sidi Bel Abbès, Sidi Bel Abbès, 22000, Algeria. ⁴Laboratoire de Physique Quantique, de la Matière et de la Modélisation Mathématique (LPQ3M), Université de Mascara, Mascara, 29000, Algeria. ⁵School of Material Sciences and Engineering, Hebei University of Technology, Tianjin, 300130, P.R. China. ⁶Beijing National Laboratory for Condensed Matter Physics, Institute of Physics, Chinese Academy of Sciences, Beijing, 100190, P.R. China. ⁷Laboratory for Developing New Materials and their Characterization, University of Setif 1, Setif, 19000, Algeria. Correspondence and requests for materials should be addressed to Z.C. (email: cheng@uow.edu.au)

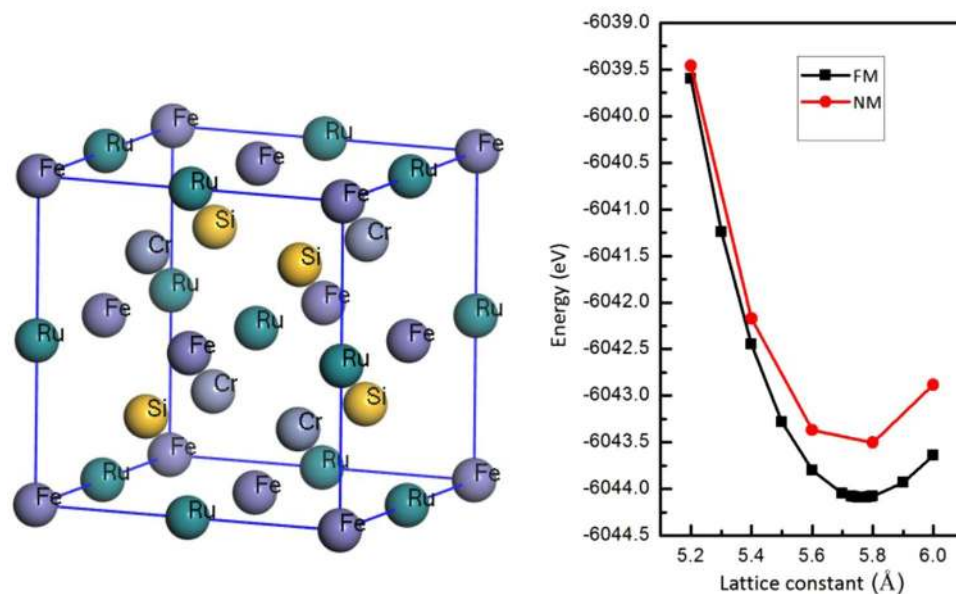


Figure 1. Crystal structure of EQH compound FeCrRuSi (left) and calculated total energies of FeCrRuSi compound with respect to the lattice constant. The NM (non magnetic) and FM (Ferromagnetic) states have been taken into account.

to the appearance of disorder. The half-metallic properties of the EQH compounds are quite robust, however, against interfering effects¹⁸. Here, we have simply reviewed the studies of the EQH compounds as follows: First, some EQH compounds XYMZ, where X, Y, and M denote the 3d transition-metal-elements, such as CoFeMnZ (Z = Al, Ga, Si, Ge)⁷, CoFeCrZ (Z = Al, Ga, Ge)¹⁰, and CoMnCrAl¹⁹, have been predicted experimentally and/or theoretically to be novel HMMs. Then, the scope of the EQH based HMMs has been extended to the compounds including 4d transition-metal-elements or rare-earth-elements, such as CoRuFeZ (Z = Al, Ga)²⁰, ZrCoTiZ (Z = Al, Ga, Si, and Ge)²¹, ZrFeVZ (Z = Al, Ga, In)²², YCoTiZ (Z = Si, Ge)²³ and YCoCrZ (Z = Si, Ge, Ga, Al)²⁴. The half-metallic/spin-flipping band gap values of these compounds are normally larger than those of the EQH compounds containing only 3d-transition-elements, which is beneficial to the stability of the half-metallicity in practical applications. Very recently, our work²⁵ demonstrates that the EQH compound LuCoCrGe can become a highly dispersive (near-linear-dispersive) zero-gap HMM at its strained lattice constant. Motivated by above-mentioned information, we must point out that the 4d-transition-elements-contained HMMs seem to be monumental treasures and worth mining.

In 2006, Mizutani *et al.*²⁶, via first-principle calculations, have investigated the HM properties and the stability of the ferromagnetic state in the $(\text{Fe}_x\text{Ru}_{1-x})_2\text{CrSi}$ ($0 \leq x \leq 1$). In 2007 and 2009, the peculiar magnetic, structural, magnetotransport and electrical behaviors of $\text{Ru}_{2-x}\text{Fe}_x\text{CrSi}$ have been reported experimentally by Hiroi *et al.*^{27,28}. In current study, we mainly focus on the interesting physical properties of the 4d-transition-elements-contained EQH based HMM FeCrRuSi. The structural, electronic, magnetic, half-metallic, mechanical, and thermodynamic properties of the new EQH compound FeCrRuSi are studied using first-principles calculations in combination with the quasi-harmonic Debye model. The effects of the uniform strain and the tetragonal distortion on the half-metallic behaviors have been also discussed. Importantly, the phase stability of this new compound has been also studied experimentally. Our current work is likely to inspire consideration of the 4d-transition-elements-contained EQH based HMMs for application in future spintronic devices.

Results and Discussion

Electronic, magnetic, and half-metallic behaviors. The Fe_2CrSi compound has been synthesized and its physical properties were investigated by Luo *et al.*²⁹. It is found that the $L2_1$ structure is energetically more favorable than the XA structure. The Fe_2CrSi compound exhibits half-metallic properties. The Ruthenium and Ferrum are in the same group of elements and have the same outermost valence electrons. When we use the Ruthenium to replace one of the Ferrum, a new EQH compound, FeCrRuSi, is achieved, as shown in Fig. 1. For the EQH compound FeCrRuSi, the Fe, Cr, Ru and Si atoms occupy the (0, 0, 0), (0.25, 0.25, 0.25), (0.5, 0.5, 0.5) and (0.75, 0.75, 0.75) Wyckoff positions, respectively.

In order to determine the ground state properties of the FeCrRuSi compound, we perform a geometry optimization by calculating the total energy per unit cell at several lattice constants in both the ferromagnetic (FM) and nonmagnetic (NM) structures. Obviously, the total energy of the FM state is lower than that of the NM one, and the obtained equilibrium lattice constant in the FM state is 5.76 Å (see Fig. 1 and Table 1). Based on the equilibrium lattice constant, the electronic band structure of the FeCrRuSi compound has been calculated and displayed in Fig. 2. The Fermi level is located in the band gap in the minority spin channel. The valence band maximum (VBM) occurs at the Γ point in the Brillouin zone and the conduction band minimum (CBM) occurs at the X

Compound	Total	Fe	Cr	Ru	Si	a (Å)	Z_t	S-P rule	P (%)
FeCrRuSi	2.00	-0.37	2.82	-0.44	-0.01	5.76	26	$M_t = Z_t - 24$	100

Table 1. Calculated equilibrium lattice constant, total and individual atomic magnetic moments (μ_B), number of valence electrons, spin polarization and possible Slater-Pauling (S-P) rule for the EQH compound FeCrRuSi.

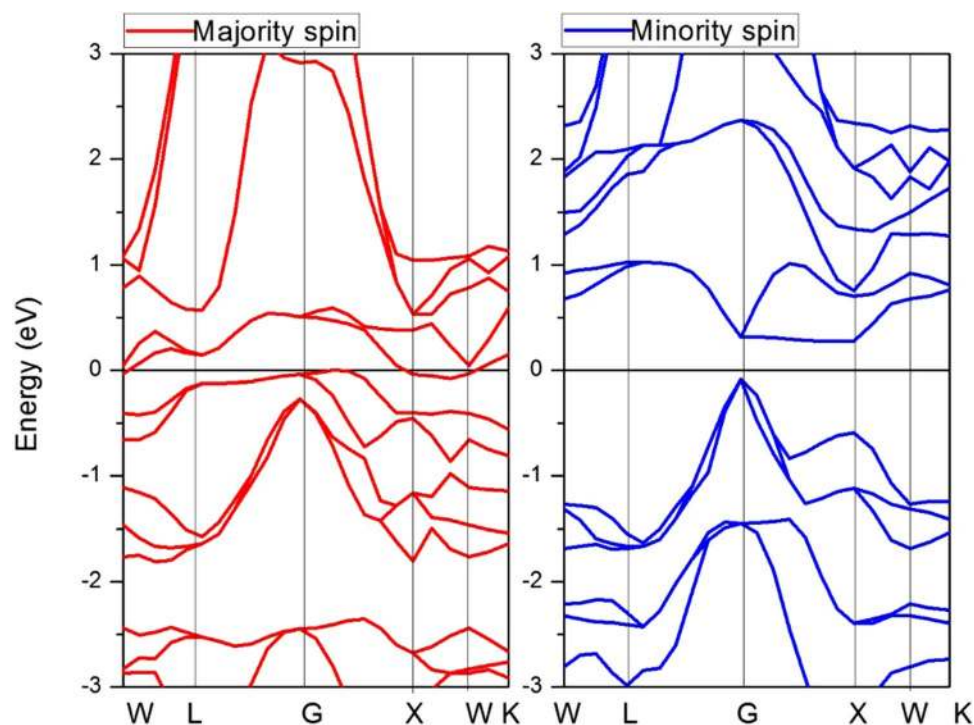


Figure 2. Calculated band structures of FeCrRuSi compound at its equilibrium lattice constant.

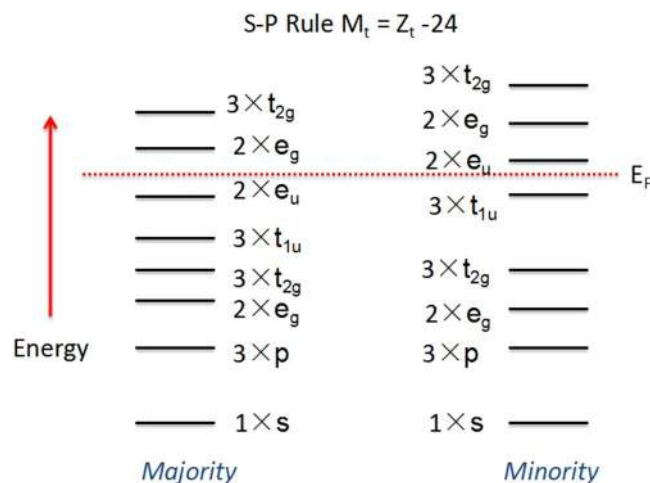


Figure 3. Schematic representation of the band structure for the FeCrRuSi EQH compound.

point in the Brillouin zone. The value of the indirect band gap is 0.384 eV in the minority spin channel. However, the majority spin band structure exhibits a metallic behavior. Hence, the EQH compound FeCrRuSi is a HMM.

Origin of the half-metallic band gap and the Slater-Pauling rule. To further analyze the origin of the band gap in the minority spin channel, we show a schematic diagram of the energy levels of the spin-up (majority-spin) and spin-down (minority-spin) band structures for FeCrRuSi in Fig. 3. In view of Fig. 3, one can see that the double degeneracy e_u states are not occupied in the spin-down channel, and therefore, a e_u (non-bonding) - t_{1u} (bonding) energy band gap is formed in the spin-down direction for this compound. Based

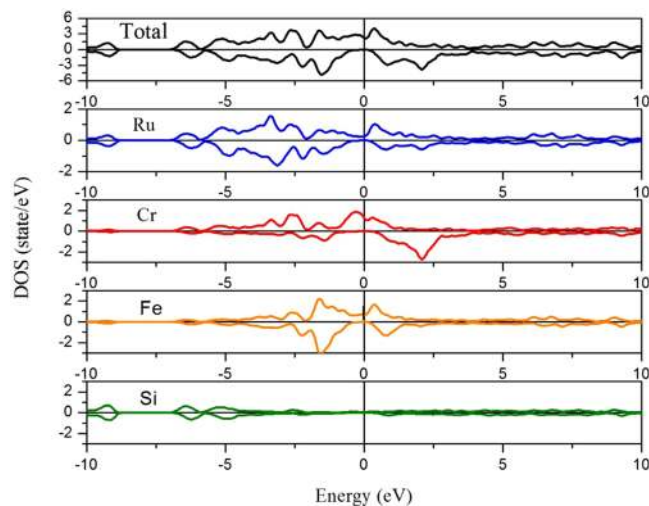


Figure 4. Calculated total and partial densities of states of FeCrRuSi EQH compound.

on the generalized electron-filling rule³⁰, for FeCrRuSi, the total number of occupied states is 14 and 12 in the spin-up and spin-down channels, respectively, and therefore, there is a total spin magnetic moment of $2\mu_B$. This theory is found to be in line with our calculated results, as shown in Table 1. Moreover, the total magnetic moment (M_t) of FeCrRuSi is an integer value, which is a typical characteristic of the EQH compounds^{25,27}. The EQH compound FeCrRuSi has 26 valence electrons (Z_v) in its equilibrium lattice, obeying the Slater-Pauling rule³¹, $M_t = Z_v - 24$. The atomic magnetic moments of the FeCrRuSi compound at its equilibrium lattice constant are also collected in Table 1. Clearly, the main contribution to the total magnetic moment comes from the Cr atoms, while the Fe and Ru atoms carry a part of the magnetic moments aligned anti-parallel to those of Cr atoms. This implies that the FeCrRuSi compound is an excellent half-metallic ferrimagnet at its equilibrium lattice constant.

We further show in Fig. 4 the calculated total and partial densities of states (TDOS and PDOS) for the EQH compound FeCrRuSi at its equilibrium lattice constant. In the minority spin channel, the bonding states of the Fe atoms mainly located in the energy around -2 eV, whereas the antibonding states of the Cr atoms mainly sited in the energy near 2.5 eV, and therefore, the corresponding bonding-antibonding states led to the formation of an energy band gap. The spin polarization (P) of the FeCrRuSi compound at the Fermi level has been calculated using the following formula:

$$P = \frac{|N \uparrow(E_f) - N \downarrow(E_f)|}{|N \uparrow(E_f) + N \downarrow(E_f)|}, \quad (1)$$

where $N \uparrow(E_f)$ and $N \downarrow(E_f)$ are the number of spin-up and spin down states, respectively. Based on the total DOS in Fig. 4, we find that the P of FeCrRuSi is 100%, reflecting that this compound could be useful for spin injection.

Effect of the strain on the magnetic and half-metallic properties. The total and atomic magnetic moments of the FeCrRuSi compound at its strained lattice constant are given in Fig. 5(a). The findings demonstrate the variation of the partial magnetic moment with respect to the contraction and the expansion of the lattice constant between 5.50 and 5.80 Å. The total magnetic moment is always equal to the fixed integer value of $2\mu_B$ at all the lattice constant values mentioned above. The magnetic moment values for the Fe and Ru atoms decrease with increasing lattice constant, whereas for the Cr atom, it continuously increases. Furthermore, in order to examine the robustness of the half-metallicity with respect to the change of lattice constant, the electronic structures of FeCrRuSi at different lattice constants (from 5.2 Å to 6.0 Å) are calculated. In this discussion, the values of the CBM and VBM for the FeCrRuSi compound in the minority spin channel have been recorded to show the half-metallic behavior for clarity, as shown in Fig. 5(b). When the value of the CBM is a positive number, and the value of the VBM is a negative number, FeCrRuSi is a HMM. But beyond that, the half-metallic behavior and the 100% spin polarization of FeCrRuSi are destroyed. From Fig. 5(b), we can observe that the half-metallic states of the EQH compound FeCrRuSi can be kept in the lattice constant value range of 5.50 – 5.80 Å. Also, the effect of a tetragonal distortion by varying the c/a ratio, with conserving the unit-cell volume, on the magnetic moments and the half-metallic properties have been investigated, as shown in Fig. 5(c) and (d). It is clear that the total and atomic magnetic moments of FeCrRuSi are nearly unchanged and the half-metallic states can be kept in the c/a ratio range of 0.96 – 1.05 .

Thermodynamic properties. To get more information about the specific behavior of a material when it is under severe constraints, e.g. high pressure and high-temperature environments, it is important to understand its thermodynamic properties. Hence, it become necessary to investigate the effects of pressure and temperature on thermodynamic parameters, such as thermal expansion coefficient α , heat capacity C_v , Grüneisen constant γ , and

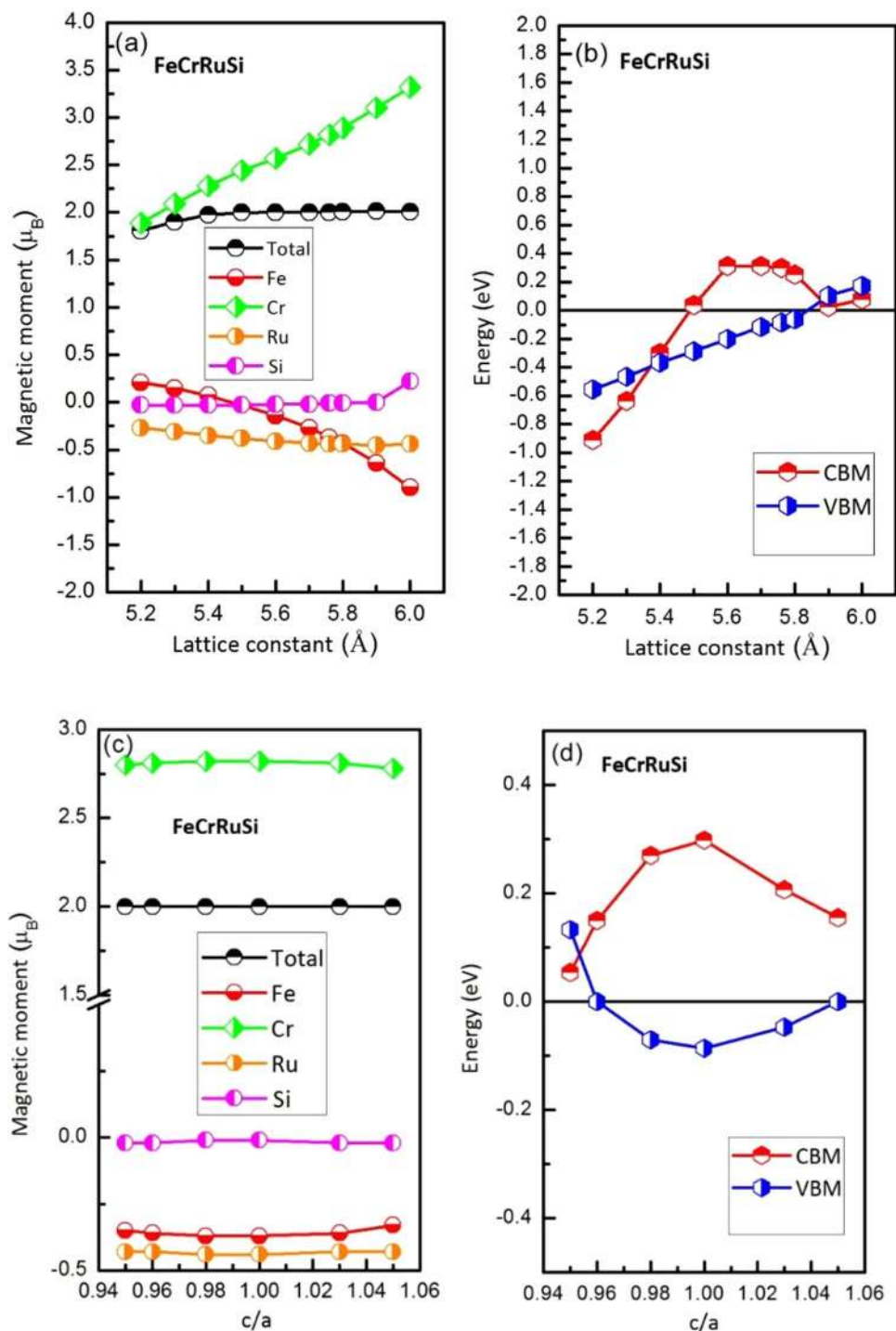


Figure 5. (a) Calculated total and atomic spin magnetic moments of FeCrRuSi as functions of the lattice constant; (b) dependence of the half-metallic states on the lattice constant (uniform strain); (c) calculated total and atomic spin magnetic moments of FeCrRuSi as functions of the c/a ratio; (d) dependence of the half-metallic states on the c/a ratio (tetragonal strain).

Debye temperature Θ_D . Here, we applied the quasi-harmonic Debye model³² to investigate the thermodynamic properties of the FeCrRuSi compound. The thermal properties are determined in the temperature range from 0 to 1200 K at some fixed pressures in the 0–45 GPa range.

In the quasi-harmonic Debye model³², the non-equilibrium Gibbs free energy of a solid is given by the following expression:

$$G^*(V; P, T) = E(V) + PV + A_{\text{vib}}(\theta_D(V); T) \quad (2)$$

where $E(V)$ is the total energy per unit cell of the material, $\theta_D(V)$ is the Debye temperature and A_{vib} is the vibrational Helmholtz free energy, which is defined as follows:

$$A_{\text{vib}}(\theta_D; T) = nkT \left[\frac{9}{8} \frac{\theta_D}{T} + 3 \ln(1 - e^{-\theta_D/T}) - D(\theta_D/T) \right] \quad (3)$$

where n is the number of atoms per formula unit, $D(y)$ is the Debye integral defined as follows:

$$D(y) = \frac{3}{y^3} \int_0^y \frac{x^3}{e^x - 1} dx \quad (4)$$

The Debye temperature of an isotropic solid can be computed as:

$$\theta_D = \frac{h}{k} [6\pi^2 V^{1/2} n]^{1/3} f(\sigma) \sqrt{\frac{B_s}{M}} \quad (5)$$

where M is the molecular mass per formula unit, B_s the static bulk modulus, which is defined by the following expression:

$$B_s = B_{\text{static}} = V \left(\frac{d^2 E(V)}{dV^2} \right) \quad (6)$$

and $f(\sigma)$ is given as:

$$f(\sigma) = \left\{ 3 \left[2 \left(\frac{2 + \sigma}{3 + \sigma} \right)^{2/3} + \left(\frac{1 + \sigma}{3 + \sigma} \right)^{2/3} \right]^{-1} \right\}^{1/3} \quad (7)$$

where σ is the Poisson ratio.

The equilibrium volume $V(T, P)$ curve (equation of state (EOS)) can be obtained from the equation:

$$\left(\frac{\partial G^*(V; P, T)}{\partial V} \right)_{P, T} = 0 \quad (8)$$

The isothermal bulk modulus B_T is defined as follows:

$$B_T(T, P) = -V \left(\frac{\partial P}{\partial V} \right)_T \quad (9)$$

where the derivative is computed at the equilibrium volume at T and P . B_T can be more conveniently expressed as:

$$B_T(T, P) = V \left(\frac{\partial^2 G^*(V; P, T)}{\partial V^2} \right)_{P, T} \quad (10)$$

The process of minimization and derivation involved in Eqs (8) and (10) is described in ref.³².

The heat capacity C_V and C_P can be calculated from the following expressions:

$$C_{V, \text{vib}} = 3nk_B \left[4D(\theta_D/T) - \frac{3\theta_D/T}{e^{\theta_D/T} - 1} \right] \quad (11)$$

$$C_{P, \text{vib}} = C_{V, \text{vib}}(1 + \alpha_V \gamma_{\text{th}} T) \quad (12)$$

where α_V represent the volume thermal expansion and γ_{th} is the thermal Grüneisen parameter, which are defined as:

$$\alpha_V = \frac{\gamma_{\text{th}} C_{V, \text{vib}}}{B_T V} \quad \text{and} \quad \gamma_{\text{th}} = - \frac{d \ln \theta_D(V)}{d \ln V} \quad (13)$$

Figure 6 shows the variation of the normalized primitive cell volume V/V_0 versus temperature at some fixed pressures for FeCrRuSi, where V is the volume of the primitive cell at pressure P and V_0 is its zero pressure equilibrium volume. The primitive cell volume increases with increasing temperature but the rate is more important for temperature range above 300 K. On the other side, as the pressure P increases, V/V_0 decreases at a given temperature, and V/V_0 at higher temperature is less than that at lower temperature at the same pressure.

The thermal expansion coefficient α has an important theoretical and experimental significance and is also essential for predicting the thermodynamic equation of state. Figure 7 presents the effect of the temperature and pressure on the thermal expansion coefficient α . It is shown that α increases (decreases) with increasing temperature (pressure). For a given temperature, the thermal coefficient α decreases strongly with increasing pressure. For a given pressure, the thermal coefficient α increases sharply with increasing temperature up to 300 K. Above this temperature, α converges to a nearly constant value at high temperature. At zero pressure and 300 K, the thermal expansion α for the studied compound is $5.97 \times 10^{-5} \text{ K}^{-1}$.

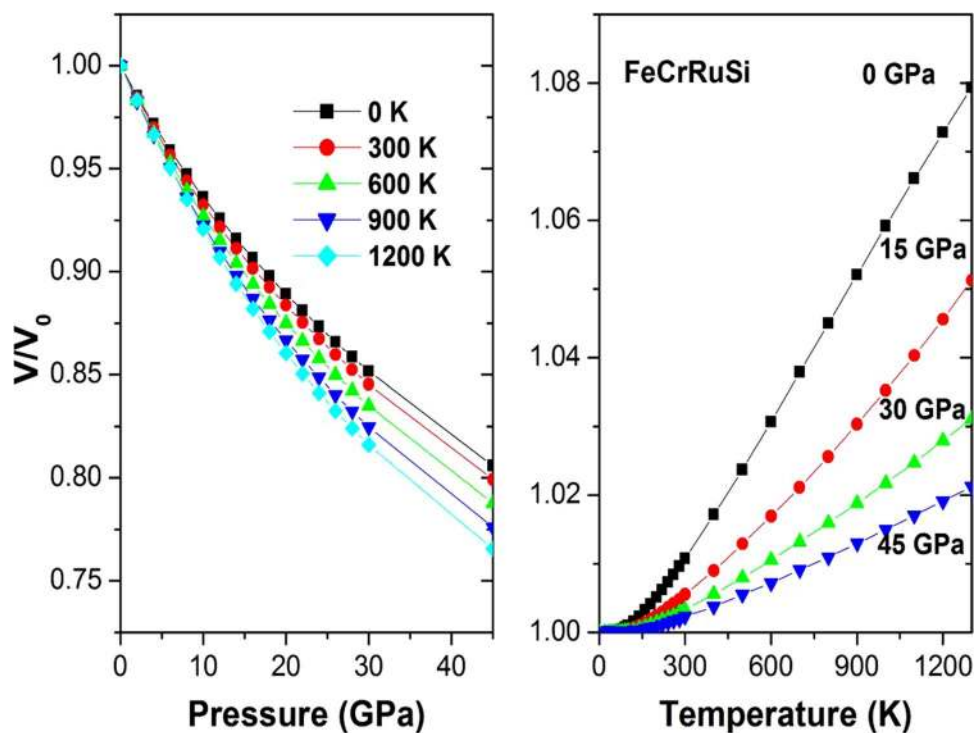


Figure 6. The normalized volume V/V_0 versus (a) pressure and (b) temperature for FeCrRuSi.

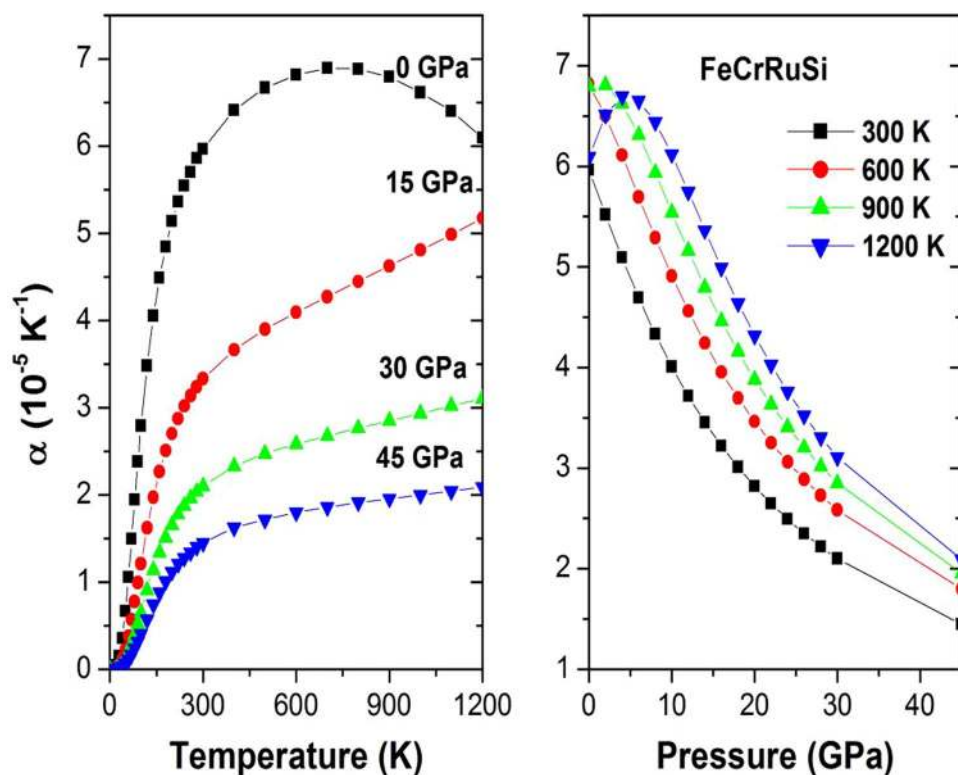


Figure 7. The thermal expansion coefficient α versus (a) pressure and (b) temperature for FeCrRuSi.

The lattice vibration properties can be accessed through the heat capacity of a material. Therefore, the heat capacity at constant volume, C_V , was calculated as a function of temperature at some fixed pressures, as shown in Fig. 8. Obviously, the C_V curve increases sharply up to 350 K, then it increases very slowly. At further high temperature C_V tends to approach the Dulong-Petit limit, indicating that the thermal energy at high temperature excites

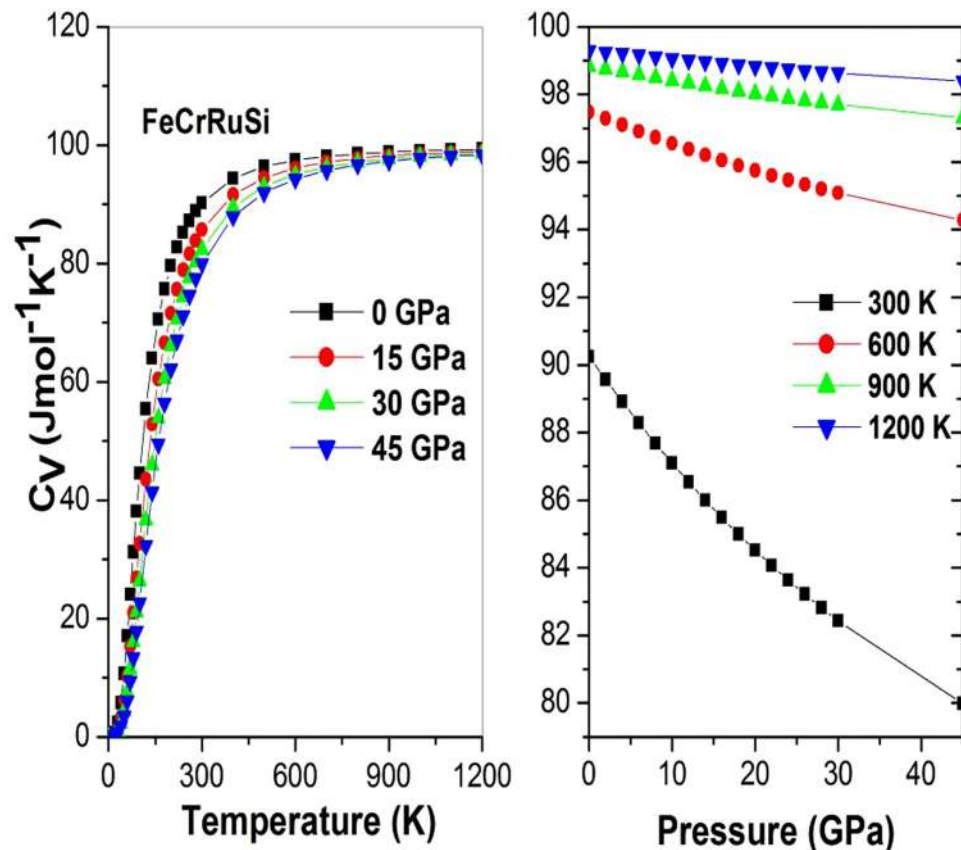


Figure 8. The heat capacity C_V versus (a) temperature and (b) pressure for FeCrRuSi.

all the phonon modes, which is common to all solids at high temperature³³. Figure 8 clearly indicates that at $T < 300$ K, the heat capacity C_V depends on both temperature and pressure (C_V is proportional to T^3)³⁴. From Fig. 8, one can note that the temperature and pressure have opposite influences on the heat capacity, and the effect of temperature on the heat capacity is more significant than that of the pressure. At high temperature C_V approaches approximately $99.51 \text{ Jmol}^{-1}\text{K}^{-1}$. At zero pressure and 300 K, the calculated value of C_V is found to be equal to $89.78 \text{ Jmol}^{-1}\text{K}^{-1}$.

The Grüneisen constant γ appears in some useful thermodynamic relations, therefore, it is significant to calculate it. Figure 9 shows the variation of the Grüneisen constant γ with temperature and pressure. It can be observed that γ is nearly constant from 0 K to 300 K, then γ increases linearly with increasing temperature. For a given temperature, γ decreases with pressure. The calculated γ of FeCrRuSi at room temperature and zero pressure is 2.353.

Finally, the evolution of Debye temperature Θ with temperature at some fixed pressures has been investigated, as shown in Fig. 10. It can be seen that Θ is nearly constant from 0 to 300 K and then decreases linearly with increasing temperature. For a given temperature, the Debye temperature increases with the enhancement of pressure. Our calculated Θ at zero pressure and ambient temperature is found to be equal to 435.14 K.

Up to now, there is no experimental data or theoretical results about the thermodynamic properties of the FeCrRuSi compound, so, our work is likely to provide a helpful reference for further investigations.

Mechanical properties. In this section, we will focus on the mechanical behaviors of the FeCrRuSi compound. Cubic crystals have only three independent single-crystal elastic constants, namely, C_{11} , C_{12} , and C_{44} . From the single-crystal elastic constants, one can calculate other important elastic moduli through the following equations³⁵:

$$B = \frac{C_{11} + 2C_{12}}{3} \quad (14)$$

$$G = \frac{G_R + G_V}{2} \quad (15)$$

$$G_V = \frac{C_{11} - C_{12} + 3C_{44}}{5} \quad (16)$$

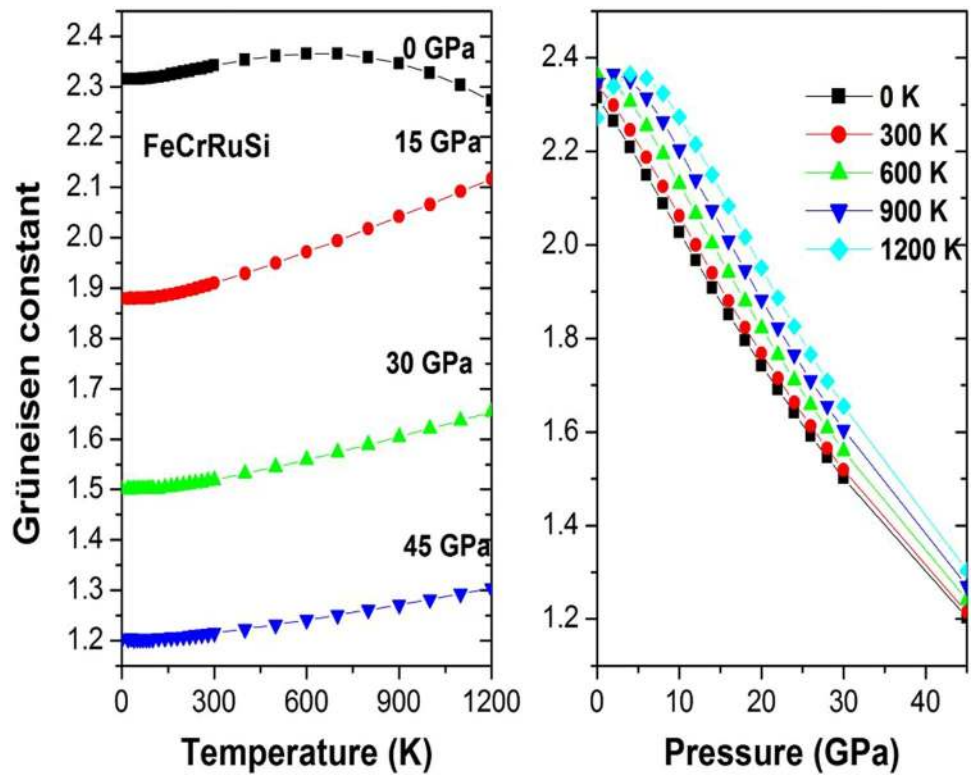


Figure 9. The Grüneisen constant γ versus (a) pressure and (b) temperature for FeCrRuSi.

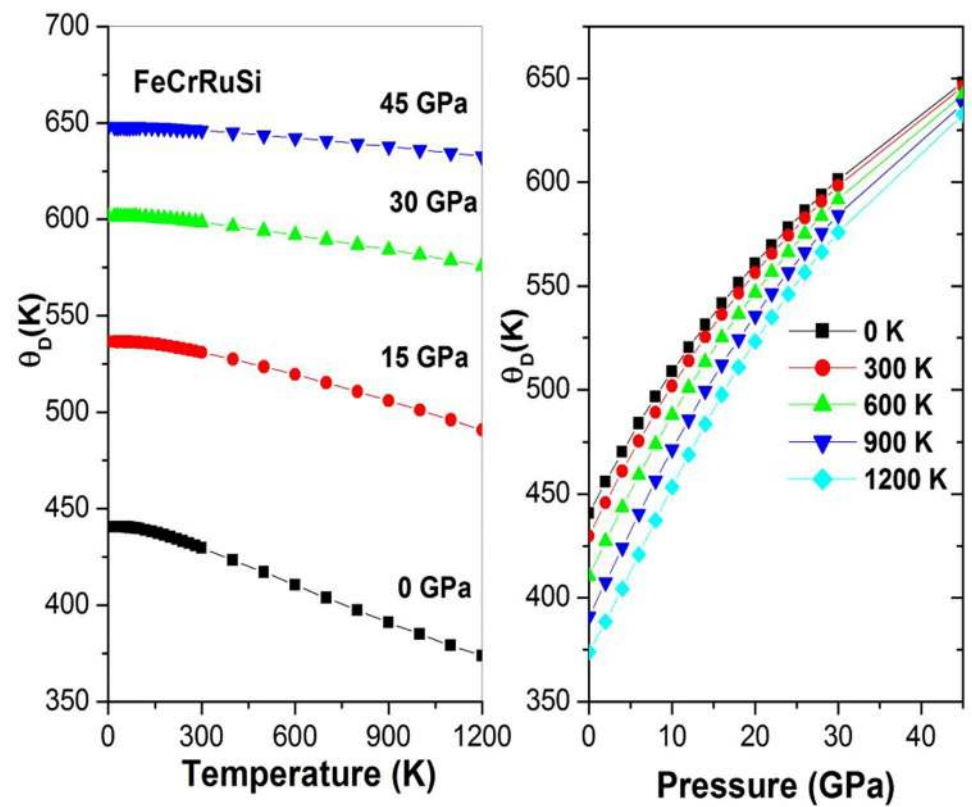


Figure 10. The Debye temperature θ versus (a) pressure and (b) temperature for FeCrRuSi.

EQH compound	C ₁₁	C ₁₂	C ₄₄	B	G	E	A	B/G	Formation energy	Cohesive energy
FeCrRuSi	361.1	181.9	141.6	241.7	121.9	239.1	1.60	1.98	-1.74	24.18

Table 2. Calculated elastic constants C_{ij} , bulk modulus B , shear modulus G , Young's modulus E (GPa), Pugh's ratio B/G , anisotropy factor A , and formation and cohesive energies (eV) for the EQH compound FeCrRuSi.

$$G_R = \frac{5(C_{11} - C_{12})C_{44}}{4C_{44} + 3(C_{11} - C_{12})} \quad (17)$$

$$E = \frac{9GB}{3B + G} \quad (18)$$

$$A = \frac{2C_{44}}{C_{11} - C_{12}} \quad (19)$$

Here, G is the shear modulus, B is the bulk modulus, G_V is the Voigt's shear modulus, G_R is the Reuss's shear modulus, E is the Young's modulus, and A is the anisotropy factor.

First, the mechanical stability of FeCrRuSi was examined according to the Born-Huang³⁶ generalized elastic stability criteria:

$$C_{44} > 0 \quad (20)$$

$$\frac{(C_{11} - C_{12})}{2} > 0 \quad (21)$$

$$B > 0 \quad (22)$$

$$C_{12} > B > C_{11} \quad (23)$$

The calculated elastic constants (Table 2) verify the mechanical stability criteria. Hence, FeCrRuSi is mechanically stable. The B/G ratio is equal to 1.98, indicating that this compound is ductile based on the Pugh's criteria³⁷. Finally, the anisotropy factor (A) has been calculated to predict the anisotropic or isotropic behavior of FeCrRuSi. As shown in Table 2, the value of the anisotropy factor A deviates from the unity, indicating that FeCrRuSi is elastically anisotropic.

Formation and cohesive energies, and phonon dispersion. In this section, the cohesive and formation energies have been calculated in order to check the structural stability of the FeCrRuSi compound. We should point out that similar analysis about the structural stabilities of Heusler compounds can be found in some references³⁸⁻⁴¹. First, we calculate the cohesive energy via the formula:

$$E_{coh}^{FeCrRuSi} = (E_{Fe} + E_{Cr} + E_{Ru} + E_{Si}) - E_{total}^{FeCrRuSi}, \quad (24)$$

where E_{Fe} , E_{Cr} , E_{Ru} , and E_{Si} are the isolated atomic energies of the Fe, Cr, Ru and Si atoms, respectively, and $E_{total}^{FeCrRuSi}$ is the total energy of FeCrRuSi per formula unit. The calculated cohesive energy is found to be equal to 24.18 eV which is very large (even larger than 20 eV), indicating the chemical stability of FeCrRuSi. The formation energy is calculated using the following expression:

$$E_f^{FeCrRuSi} = E_{FeCrRuSi}^{total} - (E_{Fe}^{bulk} + E_{Cr}^{bulk} + E_{Ru}^{bulk} + E_{Si}^{bulk}), \quad (25)$$

where $E_{total}^{FeCrRuSi}$ is the total energy of FeCrRuSi per formula unit, and E_{Fe}^{bulk} , E_{Cr}^{bulk} , E_{Ru}^{bulk} and E_{Si}^{bulk} are the total energies of the Fe, Cr, Ru and Si bulks, respectively. The calculated formation energy is equal to -1.74 eV, indicating the structural stability of the considered compound, and thus this compounds may be synthesized using conventional equilibrium methods such as arc-melting.

To further elucidate the dynamical stability of the FeCrRuSi compound, we have also calculated its phonon dispersion along the X-R-M- Γ -R directions in the Brillouin zone and the corresponding density of state (DOS) at its equilibrium lattice constant, which are displayed in Fig. 11. It is clearly seen that the phonon dispersion spectrum has no imaginary frequencies, indicating the dynamical stability of the FeCrRuSi compound.

Structural properties in experiment. In this section, we will make an outlook about the measured structural properties. Fig. S1 shows the XRD patterns of the EQH compound FeCrRuSi annealed at 773 K for 3 days. The experimental lattice constant value of FeCrRuSi is equal to 5.758 Å, which is in agreement with our calculated equilibrium lattice constant (5.76 Å). Obviously, this compound is found to exist in the EQH type (labelled also Y-type) crystal structure, however, the superlattice reflections (111) and (200) are observed to be present in FeCrRuSi. Moreover, the intensity of (200) peak is much larger and can be observed clearly, while (100) is weak,

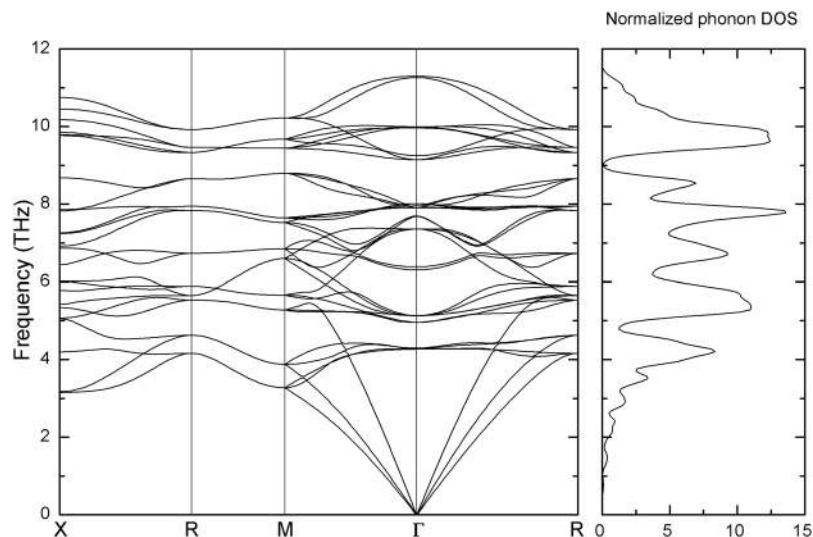


Figure 11. Calculated phonon dispersion curves and phonon DOS for FeCrRuSi at 0 GPa.

reflecting an evidence of B2 disorder⁴². Noted that, Picozzi *et al.*⁴³ reported that the half-metallic behaviors in Heusler compounds ($\text{Co}_2\text{MnGe/Si}$) can be maintained in presence of B2 disorder. The magneto-transport measurement of the FeCrRuSi compound should be performed in the follow-up work.

Summary

Using first-principles calculations and the quasi-harmonic Debye model, the structural, electronic, magnetic, half-metallic, mechanical, thermodynamic and possible Slater-Pauling behaviors of a newly designed EQH compound FeCrRuSi have been investigated in detail. Our calculation results indicate that the EQH compound FeCrRuSi is a HMM with a total magnetic moment of $2 \mu_B$ and it follows the well-known Slater-Pauling rule $M_t = Z_t - 24$. Furthermore, the origin of the half-metallic band gap of FeCrRuSi is e_u (non-bonding) - t_{1u} (bonding) energy band gap in the spin-down direction. The half-metallic behavior of FeCrRuSi can be maintained for a relatively wide range of the lattice constant variations ($5.5\text{--}5.8 \text{ \AA}$) under a uniform strain and c/a ratio variations ($0.96\text{--}1.05$) under a tetragonal distortion, respectively. The quasi-harmonic Debye model is successfully applied to examine the thermodynamic behaviors of FeCrRuSi at different temperatures and pressures. FeCrRuSi is mechanically stable according to Born-Huang elastic stability criteria. FeCrRuSi exhibits ductile and anisotropic characters. The considered EQH compound is energetically stable according to the calculated cohesive and formation energies, and phonon dispersion. Importantly, the FeCrRuSi compound has been prepared. It exists in the EQH type structure with presence of B2 disorder. The present work suggests that the EQH FeCrRuSi compound is useful in spintronic applications.

Method of Calculations

To investigate the structural, electronic and magnetic properties of the FeCrRuSi compound, we have performed first-principles calculations using the pseudo-potential plane-wave method⁴⁴ as implemented in the Cambridge Serial Total Energy Package (CASTEP) code⁴⁵. The CASTEP code is an effective *ab initio* program based on quantum mechanics. It can precisely simulate the ground structure, band structure, optical properties, magnetic properties, and so on. The interactions between the atomic core and the valence electrons were described by the ultrasoft pseudo-potential approach. The generalised gradient approximation (GGA)^{46,47} was adopted for the exchange-correlation potential. For all cases, a plane-wave basis set cut-off of 450 eV was used. A k -point mesh of $12 \times 12 \times 12$ was used in the Brillouin zone integrations. These parameters ensured good convergence of the total energy. The convergence tolerance for the calculations was selected as a difference in the total energy within 1×10^{-6} eV/atom.

Furthermore, the thermodynamic properties of this compound are predicted through the quasi-harmonic Debye model, in which the lattice vibrations are taken into account. The variation of the relative volume, thermal expansion, heat capacity, Grüneisen parameters and the Debye temperature with pressure and temperature are successfully obtained.

For the phonon spectrum of FeCrRuSi, we have employed the finite displacement method as implemented in the Vienna *ab initio* simulation package (VASP)⁴⁸ code based on the first-principles and the projector-augmented wave method (PAW)⁴⁹ within the GGA-PBE. An energy cutoff of 500 eV and a $5 \times 5 \times 7$ k -mesh in the Brillouin zone were adopted for the calculations of phonon spectrum.

It is worth to mention that the polycrystalline ingot of FeCrRuSi in this work was prepared by arc melting under a protective argon atmosphere. More details about the experimental procedure can be found in the supplementary material.

References

- Zutić, I., Fabian, J. & Sarma, S. D. Spintronics: Fundamentals and applications. *Rev. Mod. Phys.* **76**, 323 (2004).
- De Groot, R. A., Mueller, F. M., Van Engen, P. G. & Buschow, K. H. J. New class of materials: half-metallic ferromagnets. *Phys. Rev. Lett.* **50**, 2024 (1983).
- Brown, P. J., Neumann, K. U., Webster, P. J. & Ziebeck, K. R. A. The magnetization distributions in some Heusler alloys proposed as half-metallic ferromagnets. *J. Phys.: Condens. Matter* **12**, 1827 (2000).
- Graf, T., Felser, C. & Parkin, S. S. Simple rules for the understanding of Heusler compounds. *Prog. Solid State Chem.* **39**, 1–50 (2011).
- Felser, C., Wollmann, L., Chadov, S., Fecher, G. H. & Parkin, S. S. Basics and prospective of magnetic Heusler compounds. *APL Mater.* **3**, 041518 (2015).
- Kundu, A., Ghosh, S., Banerjee, R., Ghosh, S. & Sanyal, B. New quaternary half-metallic ferromagnets with large Curie temperatures. *Sci. Rep.* **7**, 1803 (2017).
- Alijani, V. *et al.* Electronic, structural, and magnetic properties of the half-metallic ferromagnetic quaternary Heusler compounds CoFeMnZ (Z = Al, Ga, Si, Ge). *Phys. Rev. B* **84**, 224416 (2011).
- Bainsla, L. *et al.* High spin polarization in CoFeMnGe equiatomic quaternary Heusler alloy. *J. Appl. Phys.* **116**, 203902 (2014).
- Alijani, V., Winterlik, J., Fecher, G. H., Naghavi, S. S. & Felser, C. Quaternary half-metallic Heusler ferromagnets for spintronics applications. *Phys. Rev. B* **83**, 184428 (2011).
- Gao, G. Y., Hu, L., Yao, K. L., Luo, B. & Liu, N. Large half-metallic gaps in the quaternary Heusler alloys CoFeCrZ (Z = Al, Si, Ga, Ge): A first-principles study. *J. Alloy Compd.* **551**, 539–543 (2013).
- Singh, M., Saini, H. S., Thakur, J., Reshak, A. H. & Kashyap, M. K. Electronic structure, magnetism and robust half-metallicity of new quaternary Heusler alloy FeCrMnSb. *J. Alloy Compd.* **580**, 201–204 (2013).
- Zhang, Y. J., Liu, Z. H., Li, G. T., Ma, X. Q. & Liu, G. D. Magnetism, band gap and stability of half-metallic property for the quaternary Heusler alloys CoFeTiZ (Z = Si, Ge, Sn). *J. Alloy Compd.* **616**, 449–453 (2014).
- Xiong, L., Yi, L. & Gao, G. Y. Search for half-metallic magnets with large half-metallic gaps in the quaternary Heusler alloys CoFeTiZ and CoFeVZ (Z = Al, Ga, Si, Ge, As, Sb). *J. Magn. Magn. Mater.* **360**, 98–103 (2014).
- Al-zyadi, J. M. K., Gao, G. Y. & Yao, K. L. Theoretical investigation of the electronic structures and magnetic properties of the bulk and surface (001) of the quaternary Heusler alloy NiCoMnGa. *J. Magn. Magn. Mater.* **378**, 1–6 (2015).
- Xu, G. Z. *et al.* A new spin gapless semiconductors family: Quaternary Heusler compounds. *EPL (Europhysics Letters)* **102**, 17007 (2013).
- Özdoğan, K., Şaşıoğlu, E. & Galanakis, I. Slater-Pauling behavior in LiMgPdSn-type multifunctional quaternary Heusler materials: Half-metallicity, spin-gapless and magnetic semiconductors. *J. Appl. Phys.* **113**, 193903 (2013).
- Bainsla, L. & Suresh, K. G. Equiatomic quaternary Heusler alloys: A material perspective for spintronic applications. *Appl. Phys. Rev.* **3**, 031101 (2016).
- Feng, Y., Chen, H., Yuan, H., Zhou, Y. & Chen, X. The effect of disorder on electronic and magnetic properties of quaternary Heusler alloy CoFeMnSi with LiMgPbSb-type structure. *J. Magn. Magn. Mater.* **378**, 7–15 (2015).
- Venkateswara, Y. *et al.* Electronic structure, magnetism, and antisite disorder in CoFeCrGe and CoMnCrAl quaternary Heusler alloys. *Phys. Rev. B* **92**, 224413 (2015).
- Benkaddour, K. *et al.* First-principles study of structural, elastic, thermodynamic, electronic and magnetic properties for the quaternary Heusler alloys CoRuFeZ (Z = Si, Ge, Sn). *J. Alloy Compd.* **687**, 211–220 (2016).
- Berri, S., Ibrir, M., Maouche, D. & Attallah, M. Robust half-metallic ferromagnet of quaternary Heusler compounds ZrCoTiZ (Z = Si, Ge, Ga and Al). *Comput. Condens. Matter* **1**, 26–31 (2014).
- Guo, R. *et al.* First-principles study on quaternary Heusler compounds ZrFeVZ (Z = Al, Ga, In) with large spin-flip gap. *RSC Adv.* **6**, 109394–109400 (2016).
- Rasool, M. N., Hussain, A., Javed, A., Khan, M. A. & Iqbal, F. Structural stability, electronic and magnetic behaviour of spin-polarized YCoVZ (Z = Si, Ge) and YCoTiZ (Z = Si, Ge) Heusler alloys. *Mater. Chem. Phys.* **183**, 524–533 (2016).
- Rasool, M. N., Mehmood, S., Sattar, M. A., Khan, M. A. & Hussain, A. Investigation of structural, electronic and magnetic properties of 1: 1: 1 stoichiometric quaternary Heusler alloys YCoCrZ (Z = Si, Ge, Ga, Al): An ab-initio study. *J. Magn. Magn. Mater.* **395**, 97–108 (2015).
- Zhang, L., Wang, X. & Cheng, Z. Electronic, magnetic, mechanical, half-metallic and highly dispersive zero-gap half-metallic properties of rare-earth-element-based quaternary Heusler compounds. *J. Alloy Compd.* **718**, 63–74 (2017).
- Mizutani, S., Ishida, S., Fujii, S. & Asano, S. Half-metallic properties and stability of ferromagnetic state in the full-Heusler alloys $(\text{Fe}_x\text{Ru}_{1-x})_2\text{CrSi}$ ($0 \leq x \leq 1$). *Mater. Transactions* **47**, 25–30 (2006).
- Hiroi, M. *et al.* Ferromagnetism and spin-glass transitions in the Heusler compounds $\text{Ru}_{2-x}\text{Fe}_x\text{CrSi}$. *Phys. Rev. B* **79**, 224423 (2009).
- Hiroi, M., Matsuda, K. & Rokkaku, T. Magnetic properties and a metal-semiconductor crossover in Heusler compounds $\text{Ru}_{2-x}\text{Fe}_x\text{CrSi}$. *Phys. Rev. B* **76**, 132401 (2007).
- Hongzhi, L. *et al.* Electronic structure and magnetic properties of Fe_2YSi (Y = Cr, Mn, Fe, Co, Ni) Heusler alloys: a theoretical and experimental study. *J. Phys. D: Appl. Phys.* **40**, 7121 (2007).
- Zhang, X. M. *et al.* Phase stability, magnetism and generalized electron-filling rule of vanadium-based inverse Heusler compounds. *EPL (Europhysics Letters)* **104**, 27012 (2013).
- Faleev, S. V. *et al.* Unified explanation of chemical ordering, the Slater-Pauling rule, and half-metallicity in full Heusler compounds. *Phys. Rev. B* **95**, 045140 (2017).
- Blanco, M. A., Francisco, E. & Luana, V. GIBBS: isothermal-isobaric thermodynamics of solids from energy curves using a quasi-harmonic Debye model. *Computer Phys. Commun.* **158**, 57–72 (2004).
- Wunderlich, B. Basics of thermal analysis. *Thermal Analysis of Polymeric Materials*, 71–188 (2005).
- Debye, P. Zur theorie der spezifischen wärmen. *Annalen der Physik* **344**, 789–839 (1912).
- Cherid, S. *et al.* Theoretical prediction of half metallic ferromagnetic full-Heusler alloys Cs_2CrGe . *Solid State Commun.* **260**, 14–18 (2017).
- Born, M., & Huang, K. *Dynamic Theory of Crystal Lattice*, Clarendon (1954).
- Pugh, S. F. XCII. Relations between the elastic moduli and the plastic properties of polycrystalline pure metals. *The London, Edinburgh, and Dublin Philosophical Magazine and Journal of Science* **45**, 823–843 (1954).
- Meng, F., Hao, H., Ma, Y., Guo, X. & Luo, H. Site preference of Zr in Heusler alloys Zr_2YAl (Y = Cr, Mn, Fe, Co, Ni) and its influence on the electronic properties. *J. Alloy Compd.* **695**, 2995–3001 (2017).
- Wang, X., Cheng, Z., Wang, J. & Liu, G. A full spectrum of spintronic properties demonstrated by a Cl_5 -type Heusler compound Mn_2Sn subjected to strain engineering. *J. Mater. Chem. C* **4**, 8535–8544 (2016).
- Gao, G. *et al.* Monolayer MXenes: Promising half-metals and spin gapless semiconductors. *Nanoscale* **8**, 8986–8994 (2016).
- Zhao, J. S. *et al.* First-principles study of the structure, electronic, magnetic and elastic properties of half-Heusler compounds LiXGe (X = Ca, Sr and Ba). *Intermetallics* **89**, 65–73 (2017).
- Bainsla, L., Raja, M. M., Nigam, A. K. & Suresh, K. G. CoRuFeX (X = Si and Ge) Heusler alloys: High T_C materials for spintronic applications. *J. Alloy Compd.* **651**, 631–635 (2015).
- Picozzi, S., Continenza, A. J. F. A. & Freeman, A. J. Role of structural defects on the half-metallic character of Co_2MnGe and Co_2MnSi Heusler alloys. *Phys. Rev. B* **69**, 094423 (2004).

44. Payne, M. C., Teter, M. P., Allan, D. C., Arias, T. A. & Joannopoulos, J. D. Iterative minimization techniques for ab initio total-energy calculations: molecular dynamics and conjugate gradients. *Rev. Mod. Phys.* **64**, 1045 (1992).
45. Segall, M. D. *et al.* First-principles simulation: ideas, illustrations and the CASTEP code. *J. Phys.: Condens. Matter* **14**, 2717 (2002).
46. Perdew, J. P. *et al.* Atoms, molecules, solids, and surfaces: Applications of the generalized gradient approximation for exchange and correlation. *Phys. Rev. B* **46**, 6671 (1992).
47. Perdew, J. P., Burke, K. & Ernzerhof, M. Generalized gradient approximation made simple. *Phys. Rev. Lett.* **77**, 3865 (1996).
48. Kresse, G. & Hafner, J. Ab-initio molecular dynamics for liquid metals. *Phys. Rev. B* **47**, 558–561 (1993).
49. Kresse, G. & Furthmüller, J. Efficient iterative schemes for ab initio total-energy calculations using a plane-wave basis set. *Phys. Rev. B* **54**, 11169–11186 (1996).

Acknowledgements

Prof. Wenhong Wang acknowledges financial support from the National Key R&D Program of China 2017YFA0206303, and National Natural Science Foundation of China, Grant No. 11574374. Prof. Zhengxiang Cheng thanks the Australian Research Council for support. Prof. Hongkuan Yuan acknowledges financial support from the Fundamental Research Funds for the Central Universities (No. XDJK2017B020) and the Natural Science Foundation of Chongqing (cstc-2017jcyjBX0035). Prof. Z.X. Cheng thanks the Australian Research Council for support.

Author Contributions

Z.X.C., R.K., and X.T.W. conceived the study. X.T.W., H.K. and R.K.G. carried out the numerical calculations. X.F.D., A.B., H.K.Y., W.H.W., L.Y.H. and L.Y.W. gave some comments. X.T.W., R.K., and H.K. wrote the manuscript. All the authors contributed to the analysis and discussion of the results.

Additional Information

Supplementary information accompanies this paper at <https://doi.org/10.1038/s41598-017-16324-2>.

Competing Interests: The authors declare that they have no competing interests.

Publisher's note: Springer Nature remains neutral with regard to jurisdictional claims in published maps and institutional affiliations.



Open Access This article is licensed under a Creative Commons Attribution 4.0 International License, which permits use, sharing, adaptation, distribution and reproduction in any medium or format, as long as you give appropriate credit to the original author(s) and the source, provide a link to the Creative Commons license, and indicate if changes were made. The images or other third party material in this article are included in the article's Creative Commons license, unless indicated otherwise in a credit line to the material. If material is not included in the article's Creative Commons license and your intended use is not permitted by statutory regulation or exceeds the permitted use, you will need to obtain permission directly from the copyright holder. To view a copy of this license, visit <http://creativecommons.org/licenses/by/4.0/>.

© The Author(s) 2017